

AperTO - Archivio Istituzionale Open Access dell'Università di Torino

Synthesis and structure determination of the novel aluminophosphate TL-1: A new layered compound with corner-sharing AlX₆ chains

This is the author's manuscript

Original Citation:

Availability:

This version is available <http://hdl.handle.net/2318/1617917> since 2018-06-12T15:34:08Z

Published version:

DOI:10.1016/j.jssc.2016.07.010

Terms of use:

Open Access

Anyone can freely access the full text of works made available as "Open Access". Works made available under a Creative Commons license can be used according to the terms and conditions of said license. Use of all other works requires consent of the right holder (author or publisher) if not exempted from copyright protection by the applicable law.

(Article begins on next page)



UNIVERSITÀ DEGLI STUDI DI TORINO

This is an author version of the contribution published on:

Questa è la versione dell'autore dell'opera:

*[Journal of Solid State Chemistry, Volume 242, Part 1, 2016,
10.1016/j.jssc.2016.07.010]*

The definitive version is available at:

La versione definitiva è disponibile alla URL:

[<http://www.sciencedirect.com/science/article/pii/S0022459616302687>]

Synthesis and structure determination of the novel aluminophosphate TL-1: a new layered compound with corner-sharing AlX₆ chains

Linda Pastero^{1,2,3}, Rossella Arletti^{1,2,3*}, Fernando Cámara^{1,2,3}, Lara Gigli^{1,2}, Monica Cagnoni⁴

¹ Dipartimento di Scienze della Terra, Università di Torino, Via Valperga Caluso 35, I-10125 Torino, Italy

² Interdepartmental Centre “Nanostructured Interfaces and Surfaces-NIS”, Via Quarello 15A, 10135 Torino, Italy

³ CrisDi - Interdepartmental Center for Crystallography, Università di Torino, Via Pietro Giuria 7, I-10125 Torino, Italy

⁴ Dipartimento di Chimica, Università di Torino, Via Pietro Giuria 7, I-10125 Torino, Italy

* e-mail: rossella.arletti@unito.it

ABSTRACT

A novel layered aluminophosphate (TL-1) has been synthesized. Crystals grow as pseudo-hexagonal thin platelets and their whole morphology depends on the synthesis conditions. The structure was solved by single-crystal X-ray diffraction using charge flipping methods. The synthesized layered material, with composition $[\text{AlPO}_4\text{F}(\text{H}_2\text{O})]-(\text{H}_{10}\text{C}_4\text{ON})_4$, crystallizes in the monoclinic space group $P2_1/a$ with $a = 9.2282(5)$ Å, $b = 6.9152(4)$ Å, $c = 14.4615(9)$ Å, $\beta = 101.57(1)^\circ$. The novel compound has corner sharing $\text{AlO}_3\text{F}_2(\text{H}_2\text{O})$ octahedral chains running along $[010]$, where fluorine atoms are at the shared apices, three oxygen atoms are shared with PO_4 tetrahedra while the sixth oxygen pertain to an H_2O molecule.

The stability field of the novel material is enclosed in the $\text{HF}/\text{Al}_2\text{O}_3$ ratio ranging between 1 and 4 and the $\text{HF}/\text{morpholine}$ ratio lower than 3. At temperature lower than 190°C , the synthesis results is a pure aluminophosphate sample (low alumina/morpholine ratio). A treatment with H_2CO_3 leads to a complete morpholine removal, as shown by *in situ* Raman spectroscopy. Powder X-ray diffraction reveals that, after morpholine extraction, the material collapses. The collapse is irreversible.

1. Introduction

AlPO_{4-n} are zeotype crystalline aluminophosphate where Si⁴⁺ and Al³⁺ ions of zeolites are replaced by strictly- alternating Al³⁺ and P⁵⁺ originating a neutral tridimensional framework. AlPO_{4-n} family was discovered in the early 80's [1], and from that moment on, many efforts have been devoted to the synthesis of materials with new properties and architectures. To date, more than 200 structure type of open framework aluminophosphate are known [2,3], including 3D zeolite-like framework and 2D or 1D anionic framework, as well. A wide range of frameworks with different dimensionality can be realized by alternating Al polyhedra and P tetrahedra, this make AlPO_{4-n} a class of very interesting materials.

Due to the extraordinary importance of the zeolite phases, the knowledge of the stability field and of the mechanisms involved in nucleation and growth of these phases is fundamental to rationalize the design and synthesis.

In this work we describe the synthesis and structure of a new layered aluminophosphate, named TL-1 (*Torino Layered-1*) originally obtained as a byproduct of the AlPO₄₋₃₄ synthesis [4]. In their paper, the authors succeeded in the synthesis of large crystals of AlPO₄₋₃₄ by tuning the levels of organic template (morpholine) and hydrofluoric acid. In fact, the presence of fluorine favors the crystallization of AlPO₄₋₃₄ but hinders the formation of large crystals. Wang et al. [4] did not characterize the byproduct obtained (layered aluminophosphate) and made just a morphological description. In the present work, the synthesis parameters were systematically changed in order to define the stability field of the layered aluminophosphate and to characterize it. The effects of some post-synthesis treatments were investigated, as well.

2. Experimental

2.1 Material Synthesis

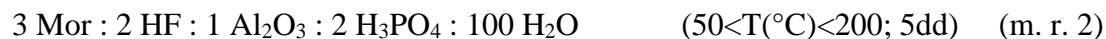
All chemicals used were Sigma Aldrich analytical grade reagents. Ultrapure water (18 MΩ) was obtained using an Elga Purelab Flex3 water purification system.

The TL-1 phase commonly occurs as a byproduct during the sol-gel synthesis of the AlPO₄₋₃₄ zeolite. The synthesis procedure followed was originally proposed by [4]. As they suggested, the templating agent used was morpholine (C₄H₉NO).

The original stoichiometry of the system, as prompted by [4], is reported in molar ratios 1.

3 Mor : 1 HF : 1 Al₂O₃ : 2 H₃PO₄ : 100 H₂O (T=200°C; 5dd) (m. r. 1)

This procedure was modified by changing the reagents molar ratio and the reaction temperatures in order to define the stability field of the new layered phase. The reference reaction for the synthesis of the new phase is reported in molar ratios 2



Water, phosphoric acid, and alumina were mixed at room temperature and stirred for half an hour. Then, morpholine and hydrofluoric acid were added to the mixture and rapidly stirred. An early reaction between morpholine and hydrofluoric acid occurs at room temperature, leading to the formation of the morpholine hydrofluoride monohydrate [5]. The presence of the precursor was confirmed by X-ray measurements and its formation was followed in-situ by Raman spectroscopy (see Raman spectroscopy section for instrumental details).

After stirring, the gel obtained was sealed in a 45 ml PTFE lined stainless steel reactor and heated in a convection oven for 5 days. The experiments were performed at a variable temperature from 50°C to 200°C. Crystals were obtained at constant temperature and autogenic pressure. After the reaction, the product was filtered, washed with ultrapure water and dried at room temperature.

2.2 Thermogravimetric analysis

TGA analysis was performed using a Seiko SSC 5200 thermal analyzer. The powder sample (10.72 mg) was loaded in a Pt crucible and heated from room temperature to 1050 °C under a constant flux of air, at a heating rate of 10 °C/min.

2.3. Single Crystal X-ray diffraction data collection and structure solution

Single-crystal X-ray diffraction was collected on an Oxford Gemini R Ultra diffractometer equipped with a CCD area detector, with graphite-monochromatized MoK α radiation. A crystal fragment of 0.115 \times 0.070 \times 0.010 mm, showing sharp optical extinction behavior was used for collecting intensity data. No crystal twinning was observed. The intensities of 9011 reflections with $-13 < h < 13$, $-10 < k < 9$, $-20 < l < 20$ were collected to 64.5° 2 θ using 1° frame width and an integration time of 73 and 7.4 s (retakes). We collected 7 ω scans, with a total of 340 frames and a detector distance-crystal of 55 mm. Data were integrated and corrected for Lorentz and polarization background effects, using the package CrysAlisPro, Agilent Technologies, Version 1.171.36.20 (release 27-06-2012 CrysAlis171.36.24). Refinement of the unit-cell parameters was based on 2647 measured reflections. At room

temperature, the unit-cell parameters are $a = 9.2282(5)$, $b = 6.9152(4)$, $c = 14.4615(9)$ Å, $\beta = 101.565(6)^\circ$, $V = 904.13(9)$ Å³, space group $P2_1/a$. The structure was solved by charge flipping methods using Superflip [6] and refined using the SHELX set of programs [6]. Details of the structural refinements, atomic coordinates, occupancy factors, equivalent isotropic thermal parameters and bond valence sums along with bond distances (Å) are reported in Tables 1, 2, and 3 respectively). Anisotropic displacement parameters and bond angles are reported as Supplementary Information (Table S1 and S2).

2.4 X-Ray Powder Diffraction data collection and refinement

X-Ray powder diffraction data (XRPD) were collected on a X' Pert PRO PANalytical diffractometer with Bragg–Brentano θ – θ geometry, equipped with a $\text{CuK}_{\alpha 1, \alpha 2}$ radiation. The spectrum was collected in the 2θ range 3 – 120° with a 0.02 step and counting times of 100s/step . Rietveld profile fitting was performed using the GSAS package [8], with the EXPGUI [9] interface. The starting coordinates used were taken from the single crystal refinement. The background curve was fitted using a Chebyshev polynomial with 19 coefficients. The pseudo-Voigt profile function proposed by [10] was applied and the peak intensity cut-off was set to 0.1% of the peak maximum. The 2θ -zero shift, scale factor, and unit-cell parameters were accurately refined. Soft-restraints were applied to the P–O distances and Al–O, Al–F (1.53 , 1.83 , 1.80 , respectively) Å) and the weight was gradually decreased, after the initial stages of refinement, up to a final weight of 100 . Observed and calculated powder pattern are reported in Fig. 1.

2.5 High Temperature powder diffraction

The thermal stability of the material was studied by *in situ* high temperature X-ray powder diffraction (HT-XRPD). Data were collected with a Philips X'Pert Pro X-Ray diffraction system equipped with a PANalytical solid state detector, operating in reflection mode, with $\text{CuK}_{\alpha 1, \alpha 2}$

X-ray data were collected over a range $5 < 2\theta < 60^\circ$ using a high temperature chamber Anton Paar HTK 1200 from room temperature up to 900°C each 50°C . Scan-step and counting time were 0.02° and 1 s/step , respectively.

2.5 Raman Spectroscopy

Raman spectroscopy was used both to verify the synthesis performance and to follow reactions *in-situ*.

The instrument used was a Labram HRVIS (Horiba Jobin Yvon Instruments) with an excitation line at 632.81 nm produced by HeNe laser at 20 mW of emission power, a Super Notch Plus filter with a spectral resolution of 1 cm^{-1} , and a grating of 600 grooves/mm. The laser spot size was focussed to 2–5 μm with a 50–100 \times objectives. 20 to 30 accumulations in the time span of 10–30 s were collected for each spectrum. Calibration was performed using the 520.6 cm^{-1} Si band.

2.7 Scanning Electron Microscopy and Atomic Force Microscopy

Scanning electron microscopy (SEM) and atomic force microscopy (AFM) analyses were carried out to obtain detailed information on the morphology and to characterize the surface topography of the new phase.

SEM imaging was performed using a Cambridge S360 microscope (operating conditions: EHT 20 to 25 kV, WD 1 to 6 mm, probe current 100 pA). Samples were sonicated for 15 minutes in ultrapure water, dropped off on conductive stubs and coated with gold in order to prevent the electron beam from charging the sample.

AFM data were collected in AC mode using a DME microscope equipped with a $50\text{ }\mu\text{m} \times 50\text{ }\mu\text{m} \times 5\text{ }\mu\text{m}$ piezoelectric probe scanner. Samples were dropped off on 4 mm cover glasses, dried at room temperature and measured ex-situ.

2.8 Wavelength Dispersive Spectrometry Electron Microprobe Analyses

A polished probe of synthesis powder dispersed in epoxidic resin was analysed with a JEOL 8200 Super Probe operating in X-ray wavelength-dispersive mode WDS mode (WDS-EMPA) with an accelerating voltage of 15 kV, a specimen current of 5 nA, and a beam diameter of 5 μm . The following standards were used: Al: synthetic almandine ($\text{Mg}_3\text{Al}_2\text{Si}_3\text{O}_{12}$); P: apatite ($\text{Ca}_5(\text{PO}_4)_3\text{F}$); F: hornblende ($\text{Ca}_2(\text{Mg,Fe})_4\text{AlSi}_7\text{AlO}_{22}\text{F}_2$). Oxygen was calculated by stoichiometry. The organic part of the unit cell content as well as the H_2O group was not analysed. The data were reduced and corrected using a Phi–Rho–Z quantitative analysis program. The results average of 5 analysis point yielded (in wt %) P_2O_5 29.64 (29.09–30.57), Al_2O_3 19.44 (18.96–20.40) and F 7.28 (7.04–7.49).

3. Results and discussion

Structure determination by single crystal diffraction

The structure of TL-1 revealed on the basis of the single crystal X-ray diffraction data consists of a aluminophosphate layers alternated along *c* axis with double organic layers constituted by morpholine cations, leading to a large interlayer distance of about 14 Å (Figure 2).

A similar situation was found in an analogous layered aluminophosphate in which the organic interlayer was constituted by 1-phenylethylamine double layer [11]. In both the cases the two layer of organic molecules are held together only by H bond interactions, leading to a plate like-morphology with clear cleavage surfaces on (001) planes.

The TL-1 layer is built by a chain of corner sharing Al octahedra running along [010] connected by PO₄ tetrahedra. Each Al is coordinated by two fluorine cations (shared with the two neighboring octahedra), three oxygen atoms (shared with the P tetrahedra) and by a water molecule (Figure 3 a, b). PO₄ tetrahedra connect the chains within the layers and are linked to three different Al octahedra, sharing with them three oxygens atoms. The fourth vertex is a non-bridging oxygen pointing at the interlayer and interacting with a strong hydrogen bond (1.68 Å) with the protonated NH₂ group of the template (Figure 2 and 3b). A similar aluminophosphate chain was found by Hawthorne (1983) [12] in natural phase tancoite, although in this case the octahedral chains are linked by (OH) groups, and each Al octahedral is surrounded by four phosphate groups. Chains are connected through bonding with Na octahedra chains sharing edges along the chain direction and with PO₄ tetrahedra. Other natural phases having this kind of chains are kastningite ((Mn,Fe,Mg)(H₂O)₄[Al₂(OH)₂(H₂O)₂(PO₄)₂].2H₂O) [13] and manganogordonite (MnAl₂(PO₄)₂(OH)₂(H₂O)₆.2H₂O) [14], which have the Al octahedra linked by (OH) groups, like in tancoite, but AlO₄(OH)₂ alternate with AlO₂(OH)₂(H₂O)₂ octahedra. The latter alternate aluminophosphate slabs with layers of independent MnO₂(H₂O)₄ octahedra and (H₂O) groups.

The bond distances found for the polyhedra are in perfect agreement with those found for other similar compounds [15-16], being the distances Al-O ranging from 1.83 to 1.856 Å, Al-F 1.81 Å and Al-O_{H₂O} 2.06 Å. The P-O distances range from 1.519 to 1.537 and are consistent with those found in other aluminophosphates, as well. The existence of an P-O terminal bond results in an anionic framework, balanced by the presence of morpholine cations in the interlayer.

The unit cell contains four morpholine molecules, distributed in a double layer, each atom of the molecule (i.e. C, O, N, H) occupy a single and crystallographic independent position. In each layer, the NH₂ groups of all the molecules are always pointing toward the non-bonding oxygen atom of the PO₄ groups, whereby is hydrogen-bonded (O4...H2B = 1.68(4) Å and H2A...O4 = 2.24(4) Å). An hydrogen bond (H1A...O7= 2.68(4) Å) is also responsible for the weak interaction between morpholine molecules of the two layers.

X ray powder diffraction experiment

To test the homogeneity of the material an XRPD refinement was provided. The full profile fitting performed with Rietveld method converged with a R/F^2 of 7.7%. The differences found between the intensity of the observed and calculated profiles reported in Figure 1 are ascribable to the preferred orientation of the powder during the sample loading. In fact, despite the use of a side loading sample holder and the efforts to avoid the orientation of the powder, an higher intensity of (001) was recorded in the pattern. Beyond that, we can conclude that the crystal structure obtained from single crystal experiment is representative of the sample.

High Temperature stability

The thermogravimetric analysis, reported in Figure 4 indicates an overall weight loss of 50.8% in the temperature range 25-1000 °C. In the first stage of heating (below 100°C) only a small weight loss of 1% is observed, probably corresponding to water molecules weakly bonded to the surface of TL-1. From the comparison of DTA and TG, two further loss are evident: 1) below 220°C (16% of weight loss) in correspondence of an endothermic reaction; 2) above 220° (33% of weight loss) in correspondence of an exothermic reaction. The first reaction is perfectly consistent with the release of the water molecules and of fluorine atoms in the structure, leading to changes in the Al coordination (from 6 to 4). The major loss of 33% observed from 220 °C to 500°C is due to the release of 3.6 morpholine molecules per unit cell in an exothermic reaction. This is strictly consistent with what found from the structural refinement (4 molecules p.u.c.). The temperature range for morpholine molecules loss is strictly in accordance with their position in the structure. The boiling point for liquid morpholine correspond to 129° C, whereas when it is present as organic template is decomposed/calcined at temperatures higher than 400°C. For example in SAPO-34 a significant fraction of products of the morpholine decomposition is eliminated at temperatures higher than 500°C due to the presence of negative charges in the SAPO-34 framework [16]. In TL-1 morpholine cations are connected to both each other and to the aluminophosphatic layer only via H-bonds, this is consistent with a release temperature between 200 and 500° C.

To test the thermal stability of TL-1 and to understand whether or not the sample could be stable or could condensate after the organic phase removal, a HT-XRPD experiment was performed.

Figure 5 shows quick XRPD patterns collected on the sample upon heating at 100, 200 and 250°C and compared with that collected at RT. The decomposition of the morpholine induce a collapse in the structure and the 00 l reflections completely disappeared. This is the consequence

of the instability of the structure after the cation removal at higher temperature, being the fourth oxygen of PO_4 tetrahedra balanced by the morpholinium cation.

Raman spectroscopy and morpholine removal

As reported in previous works [16] the main differences between the Raman spectra of morpholine in $\text{AlPO}_4\text{-34}$ and that of the liquid morpholine [17] are ascribable to the protonation of the morpholine entrapped into the framework.

In TL-1 the morpholine is present its protonated form, as well.

In Figure 6, the Raman spectra of the new phase, the $\text{AlPO}_4\text{-34}$ and the liquid morpholine are compared.

The main differences in the band positions can be summarized as follows:

- i) The band at 830 cm^{-1} (“ring-breathing vibration” of the liquid morpholine), shifts at 811 cm^{-1} in the $\text{AlPO}_4\text{-34}$ and at 827 cm^{-1} in TL-1. This shift, lower in TL-1 with respect to the $\text{AlPO}_4\text{-34}$, can be attributed to the higher degree of freedom of the morpholine arranged into the layered lattice.
- ii) The band at 1110 cm^{-1} lacks in TL-1. This band was already described in the $\text{AlPO}_4\text{-34}$ by [16], as an effect of the interaction between the morpholine and the $\text{AlPO}_4\text{-34}$ lattice. The failing of this band can be ascribed to the weak interaction between the organic and the inorganic layers of the new phase.
- iii) The stretching bands of the CH bond (between 2800 cm^{-1} and 3000 cm^{-1} in the liquid morpholine) are shifted toward lower frequencies both in TL-1 and in the $\text{AlPO}_4\text{-34}$, but in this last one the shift is larger than in TL-1. This effect can be ascribed to the interaction between the morpholine molecules and the inorganic substrate, weaker in the layered phase than in chabasitic one.

Traditional templating agent removal by heating is not advisable both for $\text{AlPO}_4\text{-34}$ and aluminophosphate because of the simultaneous leak of fluorine from the structure [18]. Structural morpholine was hydrolyzed by bubbling CO_2 into an aluminophosphate/ultrapure water suspension ($p_{\text{CO}_2}=p_{\text{atm}}$) [19-22]. This was found to be a high performance method for morpholine removal from the TL-1 structure. It was demonstrated to be effective by X-ray measurements and Raman spectroscopy, as shown in Figure 7a. The removal of the templating agent is an irreversible process.

A qualitative evaluation of the kinetics of the removal reaction was obtained by in-situ Raman spectroscopy. In particular, the area of the peak at 2958 cm^{-1} was used as a marker of the

removal reaction because of the lack of overlapping effects with other bands. From spectroscopic data, the morpholine content of TL-1 versus time decays exponentially and is completed after less than 6 hours of reaction, as shown in Figure 7b.

Stability field

Since originally obtained as a byproduct of the $\text{AlPO}_4\text{-34}$ synthesis, the identification of the stability field of the new phase is mandatory in order to promote the synthesis of the pure (layered or zeolitic) phase.

Many experiments were performed in order to define the stability field of the TL-1 phase. Few of these were discharged because not reliable, and the stability field diagrams shown in Figure 8 are based on the results of 44 runs (white-filled circles in Figure 8).

The molar ratios of the reagents ranged from 0,5 to 4 and 0,2 to 4 for $\text{HF}/\text{Al}_2\text{O}_3$ and HF/Mor respectively (Figure 8a) whereas the temperature ranged from 50°C (low-temperature conditions) to 210°C (low-hydrothermal conditions) and the $\text{Al}_2\text{O}_3/\text{Mor}$ molar ratio ranged between 0,25 and 2 (Figure 8b).

The diagrams show that the concentration of hydrofluoric acid in the system and the working temperature are the main constraints for the crystallization of the TL-1 phase.

Crystal growth and general morphology

Crystals commonly show a pseudo-hexagonal morphology. The recurring growth morphology of the crystals is dominated by the $\{001\}$ form bounded by the $[010]$ and $[110]$ directions. The low-indices facets encompassing the crystals belong to the $\{100\}$, $\{110\}$ and $\{010\}$ forms, as illustrated in Figure 9. Indices were confirmed by AFM measurements.

Both the thickness of the crystals and the whole stacking order along the $[001]$ direction strongly increase depending on the temperature that, in turn, controls the supersaturation of the system with respect to the growing crystal.

Crystals grown at high supersaturation (corresponding to high temperature) are thin and plastic, as shown in Figure 9b, where a “Dali’s melt clock”-like small aluminophosphate crystal is shown. At low temperature, corresponding to low supersaturation of the system, the overall quality of the crystals increases. The lateral facets become smooth and well developed (Figure 9d).

Experimental evidence of a change in the growth mechanism of the crystals from 2D and 3D homogeneous nucleation at high supersaturation, toward spiral growth at lower supersaturation by varying the growth temperature are obtained both at the SEM and AFM scale. In Figure 9 d),

a large spiral is detected the SEM scale. Spiral growth is the driving mechanism at low supersaturation regimes. The change in the growth mechanism, highlighted by the increase in both thickness and macroscopic stacking ordering of crystals emphasize the boundary between high and low supersaturation. At the AFM scale, when the growth mechanism turns from homogeneous nucleation to spiral growth, the {001} form starts showing periodic sequences of monolayers and macrosteps (step bouncing).

These features are limited by steps aligned along the [010] and [110] directions. The periodicity of the step sequences is ascribable to the existence of dislocations outcropping onto the {001} surface.

4. Conclusions

TL-1, anew layered aluminophosphate was obtained and characterized.

The crystal structure, as determined by X-ray diffraction, is a stacking sequence of aluminophosphate and double organic layers. The novelty of this structure is the presence of six-fold coordinated Al that form corner-sharing chains.

The templating agent can be removed by using a CO₂ saturated aqueous solution. The time required for the complete removal of the morpholine is about 6 hour.

The stability field was defined by changing the chemistry of the system and the temperature of the synthesis.

The temperature was found to deeply affect the stability and growth morphology of the crystal by controlling the supersaturation with respect to the phase.

Acknowledgements

This work was supported by the Italian MIUR, in the frame of the project FIRB 2012, Futuro in Ricerca ‘Impose Pressure and Change Technology’ (RBFR12CLQD), and by the University of Torino RICLOC 2015.... The hydrothermal growth facilities and the AFM laboratory at the Department of Earth Sciences, University of Torino were funded by Fondazione CRT (grant. N. 2014.2187 and grant N. 2014.1042).The authors are grateful to Dr Simona Bigi for the thermal analysis, and to two anonymous reviewers for their constructive reviews.

References

[1] S.T. Wilson, B.M. Lok, E.M. Flanigen. US Patent 4 (1982) 310.

- [2] L. Gómez-Hortigüela, A. Sanz, T. Álvaro-Muñoz, F. López-Arbeloa, J. Pérez-Pariente, Un-assemblable layered aluminophosphates from self-assembling structure-directing agents: Effect of fluorine, *Micr. Mes. Mat.* 183 (2014) 99-107.
- [3] J. Yu, R. Xua, Insight into the construction of open-framework aluminophosphates, *Chem. Soc. Rev.* 35 (2006) 593-604.
- [4] C. Wang, J. Wu, M. Hu, N. Li, N. Guan, S. Xiang, Synthesis of $\text{AlPO}_4\text{-34}$ and its large single crystal by partially substituting framework fluorine with oxygen species, *J. of Porous Materials* 19 (2012) 751-759.
- [5] H. Koroniak, Modzelewska, Z. Kosturkiewicz, Crystal structure of morpholine hydrofluoride monohydrate, *Pol. J. Chem.* 74 (2000) 1031-1034.
- [6] L. Palatinus, G. Chapuis, SUPERFLIP – a computer program for the solution of crystal structures by charge flipping in arbitrary dimensions, *J. Appl. Cryst.* 40 (2007) 786-790.
- [7] G.M. Sheldrick, A short history of SHELX, *Acta Cryst. A* 64 (2008) 112-122.
- [8] A.C. Larson and R.B. Von Dreele, General Structure Analysis System (GSAS), Report LAUR 86-748 Los Alamos National Laboratory New Mexico, 2004
- [9] B. H. Toby, J. EXPGUI, a graphical user interface for GSAS, *Appl. Crystallogr.* 34 (2001) 210-213.
- [10] P. Thomson, D.E. Cox, J.B. Hastings, Rietveld refinement of Debye–Scherrer synchrotron X-ray data from Al_2O_3 , *J. Appl. Crystallogr.* 20 (1987) 79-83.
- [11] R. W. Dorner, M. Deifallah , D. S. Coombes , C. R. A. Catlow , F. Corà, Synthesis and structure determination of a novel layered aluminophosphate material templated with 1-phenylethylamine: $[\text{AlPO}_4(\text{OH})](\text{NH}_3\text{C}_2\text{H}_4\text{C}_6\text{H}_5)$, *Chem. Mater.* 19 (2007) 2261-2268.
- [12] F. C. Hawthorne, The crystal structure of tancoite, *Tschermaks Min. Petr. Mitt.* 31(1983) 121-135.
- [13] G. Adiwidjaja, K. Frieze, K. H. Klaska, The crystal structure of kastningite $(\text{Mn,Fe,Mg})(\text{H}_2\text{O})_4[\text{Al}_2(\text{OH})_2(\text{H}_2\text{O})_2(\text{PO}_4)_2] \cdot 2\text{H}_2\text{O}$ -, a new hydroxyl aquated orthophosphate hydrate mineral, *J. Schluter, Zeit. Krist.* 214 (1999) 465-468.
- [14] P. B. Leavens, A. L. Rheingold, Crystal structures of gordonite, $\text{MgAl}_2(\text{PO}_4)_2(\text{OH})_2(\text{H}_2\text{O})_6 \cdot 2\text{H}_2\text{O}$, and its Mn analog, *Neues Jahrb. Mineral., Monatsh.* (1988) 265-270.
- [15] A. Tuel, C. Lorentz, V. Gramlich, C. Baerlocher, Synthesis, characterization and structure determination of two isotypes of a layered aluminophosphate with a new 2D network topology, *J. Solid State Chem.* 178 (2005) 2322-2331.

- [16] L. Marchese, A. Frache, E. Gianotti, G. Martra, M. Causa, S. Coluccia, ALPO-34 and SAPO-34 synthesized by using morpholine as templating agent. FTIR and FT-Raman studies of the host-guest and guest-guest interactions within the zeolitic framework, *Micr. Mes. Mat.* 30 (1999) 145-153.
- [17] M. Xie, G. Zhu, Y. Hu, H. Gu, Conformations of Morpholine in Liquid and Adsorbed on Gold Nanoparticles Explored by Raman Spectroscopy and Theoretical Calculations, *Phys. Chem. C*, 115 (2011) 20596-20602.
- [18] A. Martucci, A. Alberti, G. Cruciani, A. Frache, L. Marchese, H.O. Pastore, Temperature-induced transformations in CoAPO-34 molecular sieve: a combined in situ X-ray diffraction and FTIR study, *J. Phys. Chem. B*. 109 (2005) 13483-13492.
- [19] Y. Liu, R. L. Withers, L. Noren, An electron diffraction, XRD and lattice dynamical investigation of the average structure and rigid unit mode (RUM) modes of distortion of microporous AlPO₄₋₅, *Solid State Sci.* 5 (2003) 427-434.
- [20] R. J. Littel, G. F. Versteeg, W. P. M. Van Swaaij, Kinetics of CO₂ with primary and secondary amines in aqueous solutions - II. Influence of temperature on zwitterion formation and deprotonation rates, *Chem. Eng. Sci.* 47 (1992) 2037-2045.
- [21] E. Alper, Kinetics of reactions of carbon dioxide with diglycolamine and morpholine, *Chem. Eng. J.* 44 (1990) 107-111.
- [22] J. E. Crooks, J. P. Donnellan, Kinetic and mechanism of the reaction between carbon dioxide and amines in aqueous solution, *Chem. Soc., Perkin Trans. 2* (1989) 331-333.
- [23] I.D. Brown, The bond valence method: an empirical approach to chemical structure and bonding. In: *Structure and Bonding in Crystals II* (M.O'Keeffe and A. Navrotsky, editors), Academic Press, New York (1980) pp 1-30.
- [24] I.D. Brown, D. Altermatt, Bond valence parameters obtained from a systematic analysis of the Inorganic Crystal Structure Database. *Acta Cryst B*41 (1985) 244-247.

Table and Figure captions

Table 1: Details of single crystal structural refinement

Table 2. Atomic coordinates, occupancy factors, and isotropic thermal parameters of the new phase.

Table 3. Selected bond distances (Å) for the analysed sample

Figure 1: Observed (dotted line) and calculated (continuous line) diffraction patterns and final difference curve from Rietveld refinements of TL-1 (black tick marks represent Bragg reflection positions)

Figure 2. Structure of the layered aluminophosphate along [010] showing the double morpholine layer. Al octahedra shown in cyan, PO₄ groups in yellow; fluorine atoms are yellow, oxygen atoms are red. Ellipsoid represented at 50% of probability.

Figure 3: Aluminophosphate layer along a) [001] and b) [100]

Figure 4: Thermal analyses of TL-1.

Figure 5. HT-XRPD pattern collected at 25 (red), 100 (blue), 200 (green) and 250 (black) °C showing the structure collapse.

Figure 6. Raman spectra of the new layered aluminophosphate, the ALPO₄-34 and the pure liquid morpholine.

Figure 7. a) XRPD of the aluminophosphate (oriented sample) as grown (red) and after 3 hours of reaction in carbonic acid (black). The data show the collapse of the structure during the morpholine removal; b) exponential decay of the area of the peak at 2958 cm⁻¹ of morpholine shows that, after 325 minutes of reaction the morpholine removal is completed.

Figure 8. On the left, the stability field of the aluminophosphate with respect to the condensed phase (berlinite) and the zeolitic phase (ALPO₄-34) is reported. The temperature of growth is kept constant at 200°C. On the right, the stability field of the aluminophosphate with respect to the growth temperature.

Figure 9. Growth morphology of the layered aluminophosphate. a) some crystals grown at high supersaturation regime, showing 2D homogeneous nucleation onto the (001) surface; b) thin platelet showing a plastic behavior. Its morphology follows the substrate and highlights its plasticity. The crystal is 9.9 nm thick, that correspond to seven monolayers on the {001} form. The right part of the image shows a sequence of macrosteps running onto the (001) face. These macrosteps are on average 7 nm height. The thinness of the crystals can be appreciated both from AFM measurements and from their transparency to the electron beam; c) surface structure of a

spiral growing crystal; d) low temperature grown crystals. The thickness increases as the supersaturation decreases.